


FULL PAPER

Open Access



# Characteristics of the seismogenic zone in an arc-continent collision belt: insights from seismic $b$ values in Eastern Taiwan

Yu-Lien Yeh<sup>1</sup>, Bor-Yu Huang<sup>1</sup> and Strong Wen<sup>1,2\*</sup> 

## Abstract

Eastern Taiwan overlies a suture zone between the Eurasian Plate and the Philippine Sea Plate and is characterized by frequent earthquakes, often resulting in significant disasters. Notably, the region exhibits characteristics such as a high frequency of earthquakes and a short recurrence period for intense seismic events. While prior research has explored seismic  $b$  values across various periods in Taiwan, detailed investigations of the  $b$  value in the eastern region are lacking. This study employs the earthquake catalog compiled by the Taiwan Central Weather Administration to analyze spatial–temporal variations in  $b$  values in eastern Taiwan. The analysis encompasses seismic events occurring between January 1996 and June 2019. The seismic catalog is divided into three distinct time periods related to large seismic events: period I, 1996–2003 (the Chengkung earthquake); period II, 2003–2013 (the Ruisui earthquake); and period III, 2013–2019 (the Hualien earthquake). Our results indicate that most seismic events with a magnitude greater than 6 are associated with low  $b$  values. The overall  $b$  value increases during period II and then decreases substantially during period III. Although the estimated  $b$  values changed slightly, but the uncertainty in  $b$  values remained stable in this study. The epicenters of large earthquakes often overlap with areas with lower  $b$  values, especially in plate suture zones, which means that areas with lower  $b$  values usually have a higher probability of larger earthquakes. Given the extremely high potential for a catastrophic earthquake, mitigating measures should be adopted at all times.

**Keywords** Eastern Taiwan, Seismic  $b$  value, Seismogenic behavior

\*Correspondence:

Strong Wen

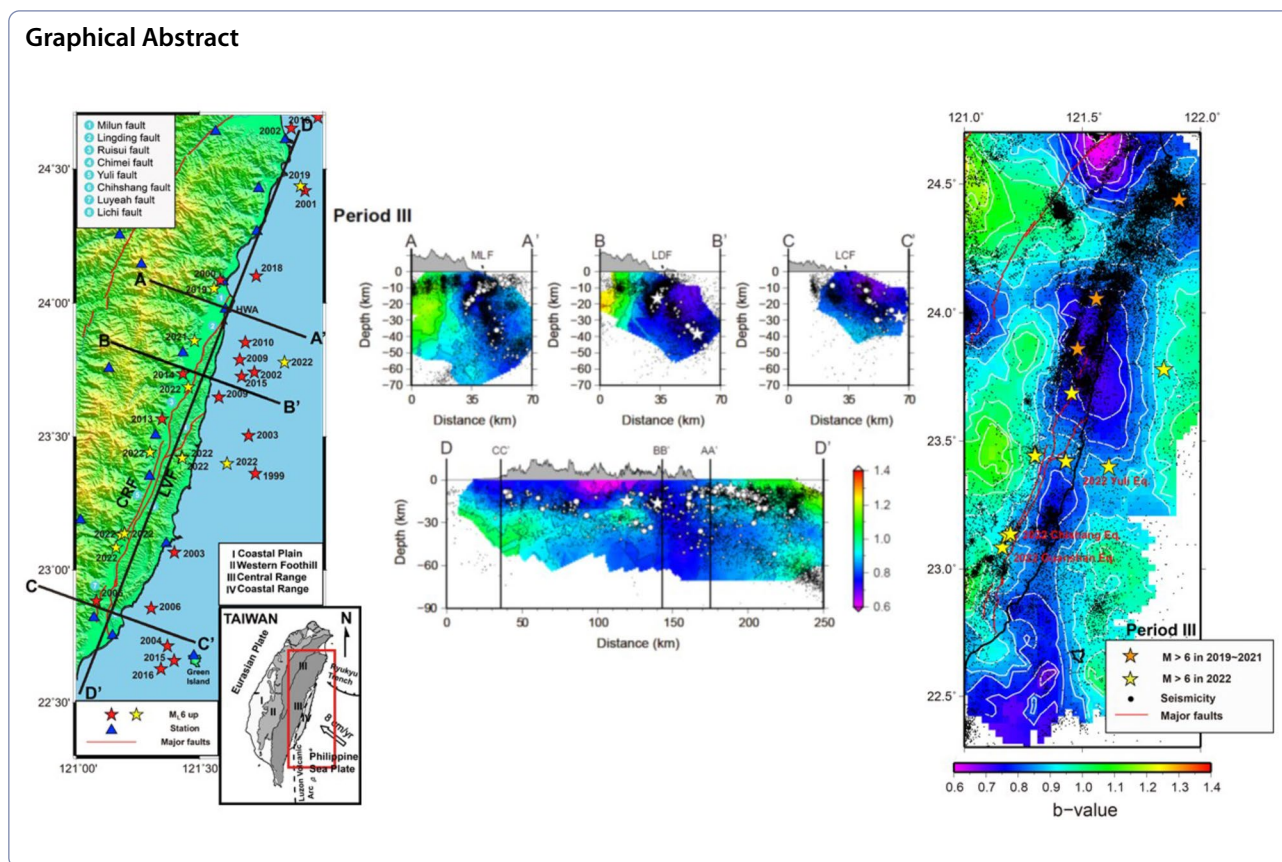
strong@eq.ccu.edu.tw

Full list of author information is available at the end of the article



© The Author(s) 2024. **Open Access** This article is licensed under a Creative Commons Attribution 4.0 International License, which permits use, sharing, adaptation, distribution and reproduction in any medium or format, as long as you give appropriate credit to the original author(s) and the source, provide a link to the Creative Commons licence, and indicate if changes were made. The images or other third party material in this article are included in the article's Creative Commons licence, unless indicated otherwise in a credit line to the material. If material is not included in the article's Creative Commons licence and your intended use is not permitted by statutory regulation or exceeds the permitted use, you will need to obtain permission directly from the copyright holder. To view a copy of this licence, visit <http://creativecommons.org/licenses/by/4.0/>.

## Graphical Abstract



## 1 Introduction

The seismic  $b$  value derived from the Gutenberg–Richter relation (1944), a fundamental parameter in earthquake studies, has been extensively employed to assess various aspects of seismic activity. It is recognized as an indicator of stress state, material properties, and fluid conditions in various tectonic regimes (e.g., Farrell et al. 2009; Gerstenberger et al. 2001; Tormann et al. 2014; Wiemer et al. 1998; Yeh et al. 2021). Furthermore, a decrease in the seismic  $b$  value serves as a precursor to a strong earthquake (Gulia et al. 2016; Nanjo and Yoshida 2018; Schurr et al. 2014; Tormann et al. 2014; Wiemer and Wyss 1997; Yeh et al. 2021), making it a crucial parameter for earthquake forecasting, and it is widely used in seismic hazard assessment (Marzocchi and Sandri 2003; Mazzotti et al. 2011). The seismic  $b$  value is negatively correlated with differential stress (Scholz 2015; Raub et al. 2017). Numerous studies have been conducted to map asperities (areas with low  $b$  values) by determining the heterogeneity of seismic  $b$  values in subducted plates and active fault zones (Chen et al. 2023; Raub et al. 2017; Sobiesiak et al. 2007; Wyss et al. 2000; Zhao and Wu 2008). Recent studies, such as those of Tormann et al. (2015) and Raub et al. (2017), have demonstrated that temporal–spatial

variations of the  $b$  value prior to and after large earthquakes can be an essential indicator of changing stress states in seismogenic zones (e.g., Yeh et al. 2021).

Taiwan is located in the vigorous collision zone between the Philippine Sea Plate and the Eurasian Plate. The region is profoundly influenced by the subduction systems of the Ryukyu Trench and Luzon Volcanic Arc and is prone to significant seismic activity (Fig. 1). Typically, for every ten seismic events that occur in Taiwan, five events occur in eastern Taiwan, according to the Taiwan Central Weather Administration (CWA) reports. The most notable and devastating earthquake in eastern Taiwan occurred in 1920, with a local magnitude  $M_L$  of 7.7 (e.g., Theunissen et al. 2010). Given such high seismic potential, understanding the seismogenic characteristics of eastern Taiwan is fundamentally important. A distinct geological feature known as the Longitudinal Valley Fault (LVF), an active suture fault of the Luzon Volcanic Arc of the Philippine Sea Plate and the Chinese continental margin of the Eurasian Plate, is present in eastern Taiwan. Earthquakes often occur along the LVF, and understanding the seismogenic characteristics of the LVF is of utmost importance. Several studies have dedicated efforts to investigating crustal deformation and segmentation to

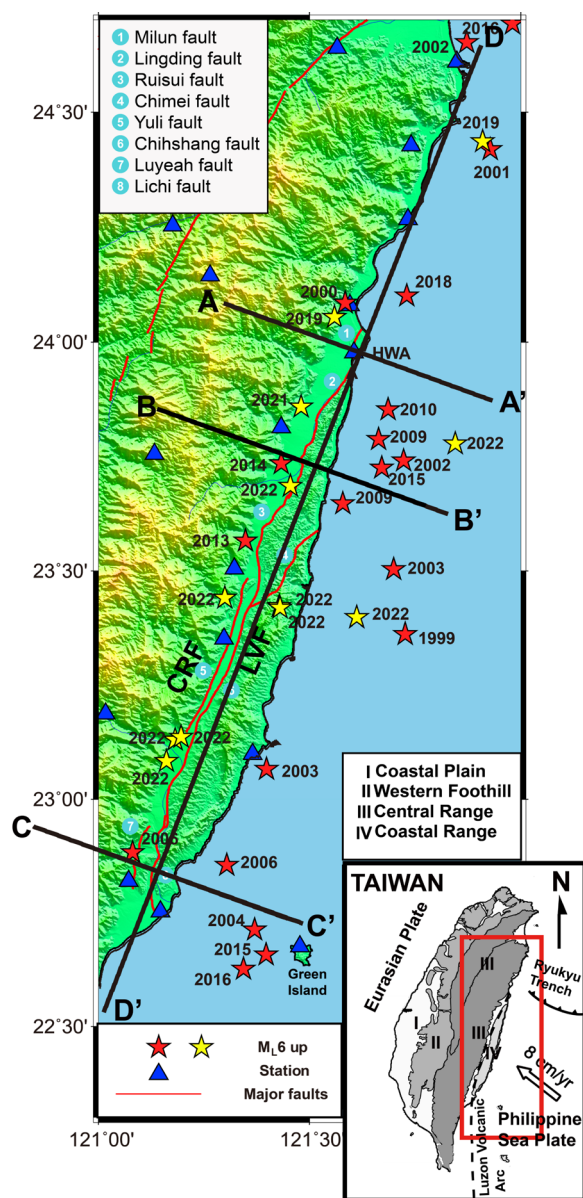


**Fig. 1** Geological setting of east Taiwan. Blue triangles represent CWASN stations. Red and yellow stars indicate seismic events with a magnitude  $\geq 6$ . Red stars denote events before the 2018 Hualien earthquake, while yellow stars represent events after the 2018 Hualien event. The red rectangle in the inset map outlines the study area. The red solid lines indicate major faults in the study area

characterize seismogenic features along the LVF (Yu and Kuo 2001; Peyret et al. 2011; Chen et al. 2020). Numerous geoscience researchers (Chan et al. 2012; Chen et al. 2023; Cheng and Yeh 1989; Hui et al. 2020; Kim et al. 2005; Tsai et al. 1981; Wang 1988; Wang et al. 2015, 2016; Wen et al. 2022; Wu et al. 2013) have investigated the  $b$  value of earthquakes in different periods for the whole or

part of the Taiwan region, yielding  $b$  values ranging from 0.8 to 1.2 (Wu et al. 2018). In recent years, with technological advancements, both the quality and quantity of earthquake recordings have increased annually. To comprehensively grasp the latest information regarding areas where earthquakes may cause damage and what countermeasures may be implemented to mitigate earthquake-induced disasters, this study utilizes the earthquake catalog compiled by the CWA. Based on the seismic  $b$  value theory proposed by Gutenberg and Richter (1944), our primary objectives are to identify the spatial distribution characteristics of  $b$  values in eastern Taiwan and to analyze variations in  $b$  values to understand the tectonic structure and the relationship between  $b$  values and seismogenic zones. Finally, we will integrate and compare studies from other fields of geological science, aiming to enhance understanding of the geology, earthquakes, and  $b$  values in eastern Taiwan and provide constructive information for future earthquake disaster prevention.

From the results of geodetic and geological data analysis, the northern segment of the LVF is identified as a locking zone (Huang et al. 2010), encompassing the Milun Fault (MLF) and the Lingding Fault (LDF). The most recent significant earthquake in this area was the 2018 Hualien earthquake ( $M_L$  6.2). In contrast, the southern segment functions as a creeping zone during inter-seismic periods and includes the Chihshang Fault (CSF), Lichi Fault (LCF), and the Luyeah Fault (Fig. 1). The most noteworthy earthquake in this segment was the 2003 Chengkung earthquake. The central segment of the LVF, where the Yuli Fault (YLF) and the Ruisui Fault (RSF) occur, experiences fewer earthquakes (Fig. 1). The suture zone between the Eurasian Plate and the Philippine Sea Plate occurs in the center of the study area, where sedimentary rocks and alluvial sediments predominate. The northern region of the LVF is governed by a reverse faulting mechanism with a left-lateral slip component along the northeast–southwest direction. The CSF (in the central part of LVF) has been responsible for several large earthquakes in the past, such as the 1951 Hualien–Taitung earthquake sequence (Cheng et al. 1996), 1990 Hualien earthquake sequence (Lee et al. 2011). However, after these significant earthquakes, the CSF’s inter-seismic activity mode has been dominated by creeping in the shallowest part of the crust around 2 km, as is still the case. The CSF is part of a submerged active fault exhibiting non-coseismic deformation and rupture. In other words, the deformation and rupture occur very slowly without an earthquake, continuously releasing energy. According to GPS data, the CSF and the entire LVF contribute 24% and 37%, respectively, of the total compression of Taiwan between the two plates, with a shortening rate of 2–3 cm/yr (Angelier et al. 2000). Geodetic survey



results and earthquake locations suggest that the northern section of the Longitudinal Valley (LV) is associated with sliding extension (in a NE–SW direction), parallel to the plate boundary, while the southern section experiences collision and extrusion perpendicular to the plate boundary (NW–SE direction) (Yu and Lee 1986).

Due to the impact of the arc-continent collision, the eastern Taiwan is subjected to immense stress, causing

the strata to deform easily and fracture with dislocations, leading to earthquakes. Consequently, earthquakes are frequent and strong in this area, as seen in the 2003 Chengkung earthquake ( $M_L$  6.4), the 2013 Ruisui earthquake ( $M_L$  6.4) in Hualien, and the 2018 Hualien earthquake ( $M_L$  6.2) off the coast of Hualien. According to the CWA report, the 2018 Hualien earthquake appears to have triggered a series of subsequent earthquakes with  $M_L > 6$  up until 2022 (Fig. 1 and Table 1). Therefore, this study is particularly concerned with the impact of seismic activity in the LV before 2018 on subsequent earthquake ruptures. Figure 2 depicts seismicity, depth histogram and energy distribution in east Taiwan. The energy is derived by converting magnitude using the equation (Okal 2019):

$$\log E = 11.8 + 1.5M_L$$

where  $E$  (in ergs) is the energy and  $M_L$  is the local magnitude.

Most of the observed seismic events occur along the collision boundary and the LVE, resulting in the highest energy release in these locations. Furthermore, in this study, we aim to investigate the spatiotemporal distribution of seismic  $b$  values to infer their relation to the seismogenic characteristics of the LVE. Analyzing the short-to-medium-term variations of the seismogenic

**Table 1** Seismic events with a magnitude greater than 6 occurred in the study area after 2018

Date	Time	Lat	Lon	Depth (km)	$M_L$
2019-04-18	05:01:07.11	24.0543	121.5592	20.33	6.32
2019-08-07	21:28:03.56	24.4363	121.9097	24.15	6.24
2021-04-18	14:14:37.80	23.8592	121.4800	14.42	6.26
2022-03-22	17:41:38.85	23.3985	121.6118	25.73	6.70
2022-03-22	17:43:25.40	23.4230	121.4277	22.63	6.21
2022-03-22	20:29:59.12	23.4190	121.4300	22.57	6.04
2022-06-20	01:05:07.78	23.6855	121.4543	7.00	6.09
2022-09-17	13:41:19.11	23.0840	121.1608	8.61	6.60
2022-09-18	05:19:19.39	23.1305	121.1817	12.13	6.15
2022-09-18	06:44:15.25	23.1370	121.1958	7.81	6.83
2022-09-19	02:07:45.11	23.4410	121.2995	13.38	6.02
2022-12-15	04:03:16.42	23.7787	121.8450	16.30	6.51

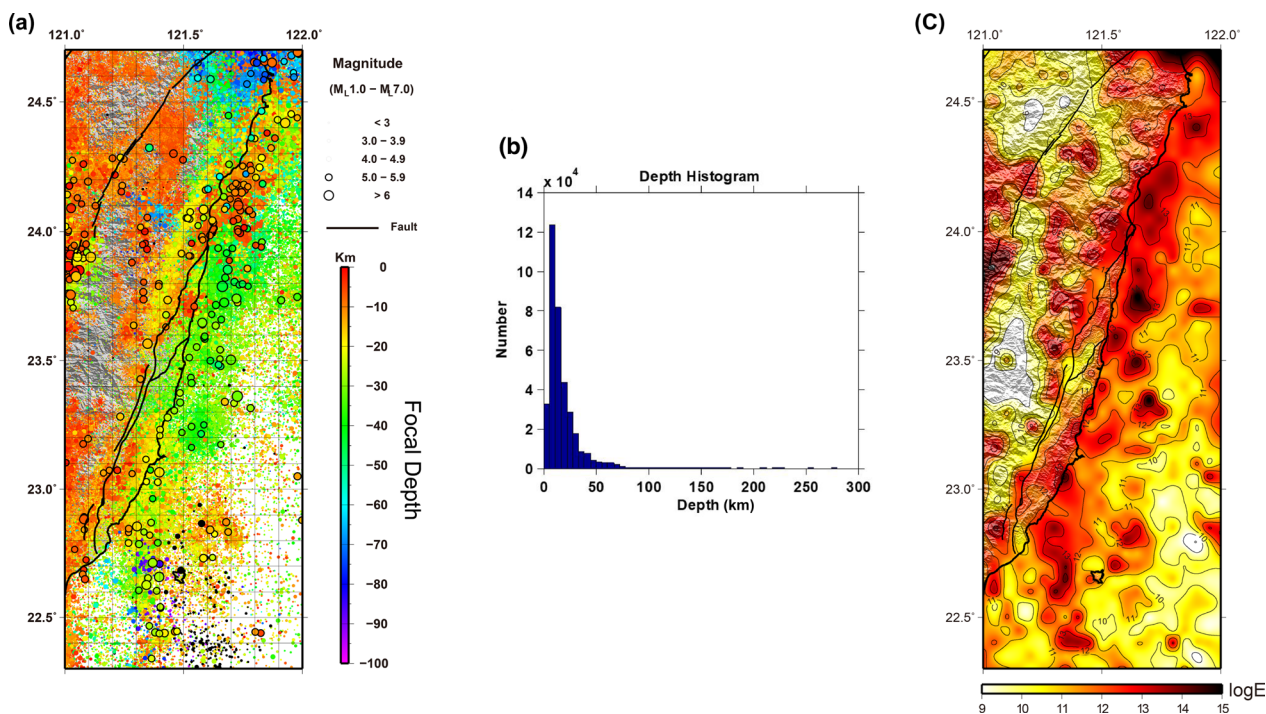


**Fig. 2** **a** Seismicity in eastern Taiwan from January 1991 to June 2019, **b** statistical map of focal depth and number of earthquakes in eastern Taiwan. The horizontal axis represents the earthquake depth, and the vertical axis represents the number of earthquakes ( $\times 10^4$ ) and **c** energy distribution in eastern Taiwan



zone in eastern Taiwan during seismic activity is beneficial for assessing future earthquake hazard potential.

## 2 Data and analysis

Conducting seismic *b* value research necessitates meticulous consideration of the impacts of clustered events and aftershocks accompanying significant earthquakes. Failure to account for these dependencies in the original earthquake catalog may yield distorted results, undermining the representativeness of seismic *b* values as an evaluative metric. To distinguish such dependencies from independent seismic activity and thus mitigate this issue, a declustering step is necessary prior to seismic *b* value analysis to eliminate the influence of repeated events, particularly aftershocks.

The seismic *b* value, according to the Richter and Gutenberg Law (1944), is expressed as

$$\log N = a - bM$$

where *N* is the cumulative number of events with a magnitude greater than *M*, and *a* and *b* are constants. The constant “*a*” is related to the seismicity of a region and “*b*” is known as seismic *b* value. The ZMAP software package, developed by Wiemer (2001), was employed for deriving the distribution of seismic *b* values. Initially, we applied the declustering technique proposed by Reasenberg (1985) to the seismic catalog to eliminate the effects of clustered events and aftershocks associated with large events. Given that aftershocks do not adhere to the Poisson distribution within a small region and over a short period, their removal from an earthquake sequence is necessary. After eliminating clusters and aftershocks, a catalog of independent earthquakes was obtained (see Fig. 3a, b). The input parameters for removing clusters and aftershocks are outlined as follows. The forecast time

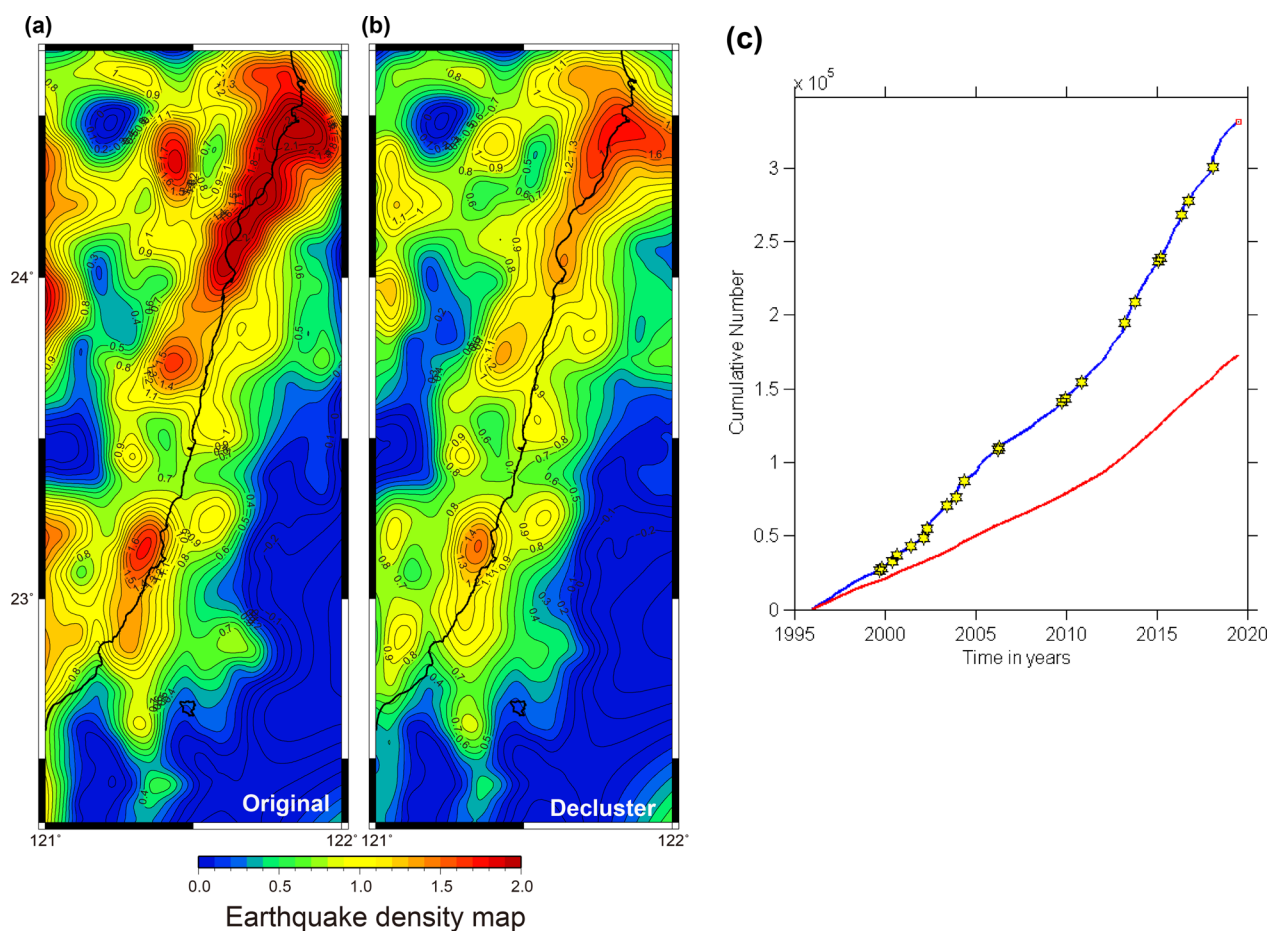


**Fig. 3** **a** Seismicity before (left panel) and **b** after (right panel) declustering. The scale number is the logarithmic value of the number of earthquakes per square kilometer. **c** Relationship between the cumulative number of earthquakes and time from January 1996 to June 2019. The horizontal axis in the figure is time, and the vertical axis is the cumulative number of earthquakes. The blue (before de-clustering) and red (after de-clustering) solid lines are the cumulative earthquake events at the corresponding time. The yellow asterisk marks earthquake events with the magnitude greater than 6

for non-cluster events was set at 1 day, and the maximum forecast time for cluster events was 10 days. Especially in Reasenber (1985), the formula (14) for confidence interval  $P=0.95$ , since it is proportional to time  $t$ , the time that must be waited to observe the next event in the sequence with reasonable confidence is infinite. An ideal upper limit for (for large  $t$ ) would be a value inversely proportional to the local background rate of seismicity. However, in this formula, a fixed limit of <10 days is used. These simplifications are made for computational efficiency and appear to have little impact on the results. Actually, it is not easy to determine the forecast time of an earthquake. Several studies (Mignan 2015; Reasenber 1985) had shown that the aftershocks of earthquakes with  $M \geq 3$  last for about 10–12 days. Therefore, this study tested different forecast times, but based on past analysis experience, 10 days is still an appropriate value. A clustered event was defined as an earthquake sequence with long-term aftershocks, with a detection probability for the next event in the sequence set at 0.95, and the effective minimum magnitude of completeness of the earthquake catalog was 1.5. For the spatial definition range of seismic clusters, the interaction radius among related earthquake events was set at 10 km with the epicenter error is 1.5 km, and the focal depth error is 2 km (Wiemer 2001). Figure 3a, b illustrates the distribution of events before and after the declustering procedure. In the figures, the earthquake density increases as the color gradually shifts to red, and vice versa. The scale number represents the logarithmic value of the number of earthquakes per square kilometer. Besides, looking at the relationship between the cumulative number of earthquakes and time (see Fig. 3c), we can see that the cumulative number of earthquakes increases roughly linearly with time. From this, we can conclude that the earthquake catalog in the study area has high integrity.

The minimum magnitude of completeness ( $M_c$ ) is a very important parameter in  $b$  value estimation.  $M_c$  is defined as the effective minimum magnitude at which 100% of earthquakes are detected across temporal and spatial scales, and it is very important to estimate this parameter because it has practical significance in the analysis of seismic activity, particularly for calculating seismic  $b$  values (Wiemer and Wyss 2000; Yadav et al. 2009). The determination of  $M_c$  is often contingent upon the seismograph density within an area; the greater the density, the greater the ability to detect smaller earthquakes.  $M_c$  also exhibits temporal variations influenced by changes in observational instruments and earthquake catalogs. Therefore, a systematic analysis of the earthquake catalog was carried out. To assess the reliability of the earthquake catalog used in this study, the maximum curvature method, referred to as the MAXC method

(Wiemer and Wyss 2000), was employed to calculate the spatial distribution of  $M_c$  as it is fast and straightforward (Wiemer and Wyss 2000). We should take a note of that the MAXC method usually underestimate the  $M_c$  as mentioned in Zhou et al. (2018), which may lead to underestimate  $b$  values, with uncertainties varying between 0.2 and 0.04. We reasoned that only enough sample sizes would allow reliable estimates of  $M_c$  to be obtained. The temporal and spatial distribution of  $M_c$  are illustrated in Fig. 4.

We applied the spatial grid analysis technique proposed by Wiemer and Wyss (2000) to the earthquake catalogue compiled by the CWA from January 1996 to June 2019 for seismic  $b$  value estimation. An appropriate grid spacing was selected, and the study area was divided into equal spacings of  $0.1^\circ \times 0.1^\circ$  grid elements. By designating the center point of each grid cell as the center of a circle and selecting earthquakes larger than  $M_c$  within a certain radius to represent the seismicity of each grid cell. By trying various radiuses to test the uncertainty of estimated  $b$  values, this research finally derived a constant radius of  $R=7$  km to identify seismic events, and the calculated  $b$  value is basically consistent with the surface geometry of the fault rupture zone, which can meet the needs of analyzing  $b$  value and stress changes. To stabilize the calculation results, the number of earthquake samples larger than  $M_c$  in each grid was at least 50. Subsequently, we used the maximum likelihood method to estimate seismic  $b$  values. Furthermore, the bootstrapping approach (bootstraps=1000) was used in the uncertainty test. Moreover, the estimated value was taken as the maternal sample for multiple repeated sampling, which gave a highly reliable seismic  $b$  value. If the number of qualified seismic samples in a grid was less than 50, seismic  $b$  value calculation was not performed due to low reliability, and the result is displayed as blank on the  $b$  value distribution map.

The original earthquake events totaled 358,158 within the study area. After excluding earthquake clusters and repeated events, 171,913 independent earthquakes were included in this study. To prevent outlier or low-quality data from affecting  $b$  value estimation, the depth and time of the earthquakes were carefully screened. In the selection of the depth segment, considering that seismic events in the study area are primarily concentrated in the depth range 0–40 km (see Fig. 2b), only a small number of earthquakes are below 40 to 70 km. Since earthquakes with less than 40 km are in great proportion, we then only discuss the  $b$  value estimation less than 40 km. To investigate seismic  $b$  values and potential seismogenic belts in the shallow and extremely shallow strata, we focused on the time period delineated by the variations of  $M_c$  over time (see Fig. 4). Before 1996,  $M_c$

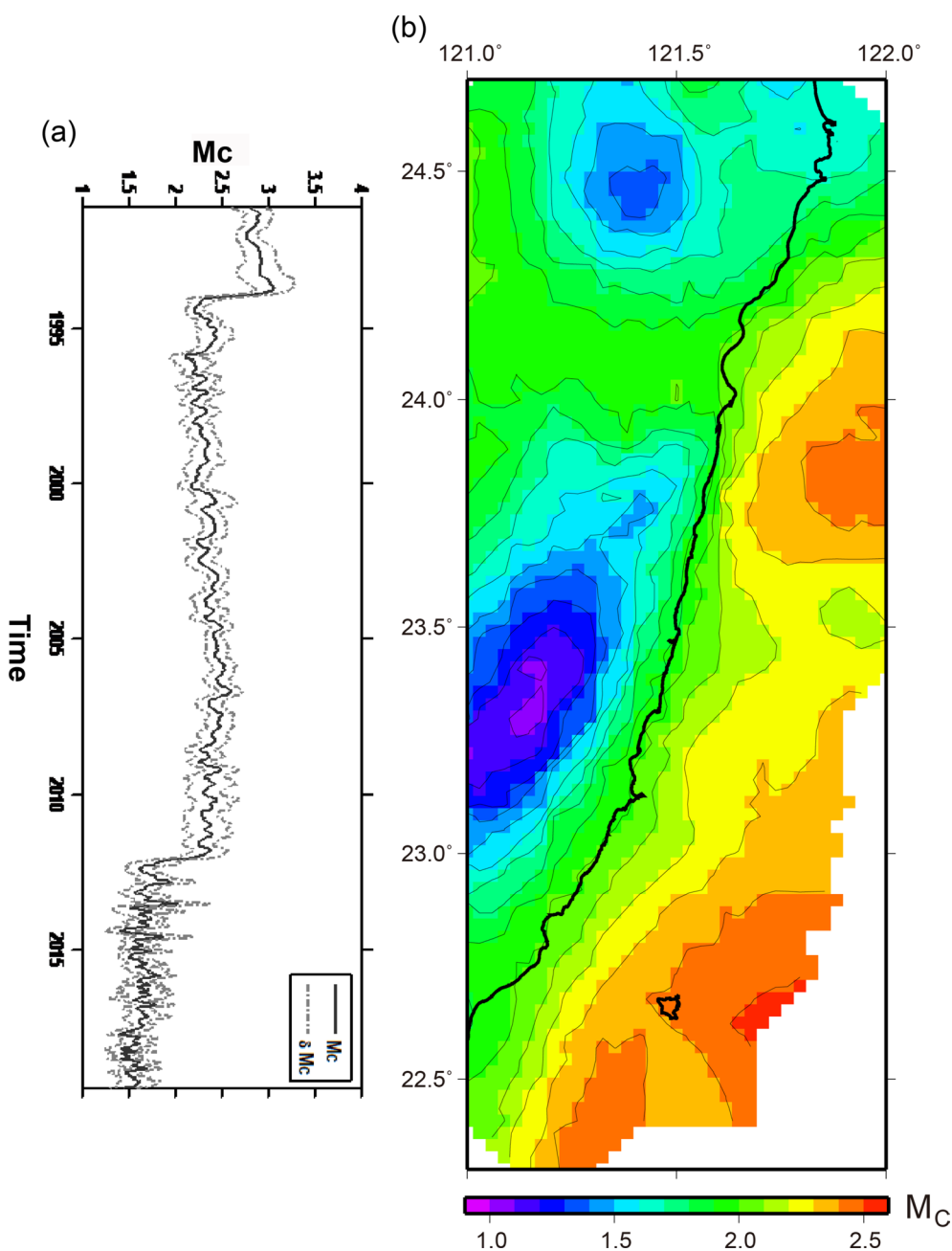


**Fig. 4** a Temporal variations and b spatial distribution of  $M_c$  used to estimate  $b$  values in the study area

exhibited a relatively large range, fluctuating between 2 and 3. This was caused by the low density of recording instruments, limiting their ability to detect small earthquakes. From 1996 to 2011, with the replacement of older seismometers and the increasing density of seismic stations,  $M_c$  ranged between 2 and 2.5. Moreover, the variation tends to be gentle. After introduction of the high-precision seismograph with a 24-bit dynamic range in 2012,  $M_c$  values were lower than 2, and the ability to

detect small-magnitude earthquakes improved substantially. To ensure that a significant variation in  $M_c$  does not affect seismic  $b$  value estimation, this study exclude seismic events with a smaller  $M_c$  in the period from January 1996 to June 2019 in the earthquake catalog. The catalog was divided into three time periods according to their temporal occurrence associated with large seismic events: (I) 1996/01–2003/03, prior to the 2003 Chengkung earthquake (10 December 2003,  $M_L$  6.4); (II)



2003/03–2013/03, prior to the 2013 Ruisui earthquake (31 October 2013,  $M_L$  6.4); (III) 2013/03–2019/06, before and after the 2018 Hualien earthquake (6 February 2018,  $M_L$  6.2). One of the reasons that we divided different time intervals to calculate  $M_c$  and  $b$  values in each period is to keep the earthquake catalog relatively uniform, thus the  $M_c$  in each period can fit well. This is also guaranteed to reduce the effect of  $M_c$  underestimation using the ZMAP.

### 3 Results and discussion

As indicated by the distribution map of Taiwan’s seismic  $b$  values at 0–10 km and 10–20 km (Wu et al. 2018), the seismic  $b$  values in the eastern Taiwan area are relatively low, ranging from 0.6 to 1.1 on the north side of the Central Mountain Range (CMR). In addition, Chan et al (2012) and Wang et al. (2015) noted that the average seismic  $b$  value in eastern Taiwan is approximately 0.9.

Chan et al (2012) obtain the  $b$  value in the source areas of large earthquakes is around 0.90–0.93. Therefore, the value of 0.9 is suitable and applicable for east Taiwan. In this study, a  $b$  value less than 0.9 is termed a low  $b$  value, while a  $b$  value greater than 0.9 is referred to as a high  $b$  value. The seismic energy map of the study area (Fig. 2b) reveals a high-energy area extending along the eastern coastline of Taiwan, which is consistent with the collision boundary of the two plates. Thus, large earthquakes often occur in this zone. In addition, this region is an area with frequent stress accumulation and release.

#### 3.1 Temporal variations of seismic $b$ values

Figure 5a–c illustrates the overall average  $b$  values for each period, while Fig. 5d presents the statistical results of estimating  $b$  values in each period. Analyzing the distribution of these three time periods (with a depth range of 0–70 km), the distribution of  $b$  values exhibits a high

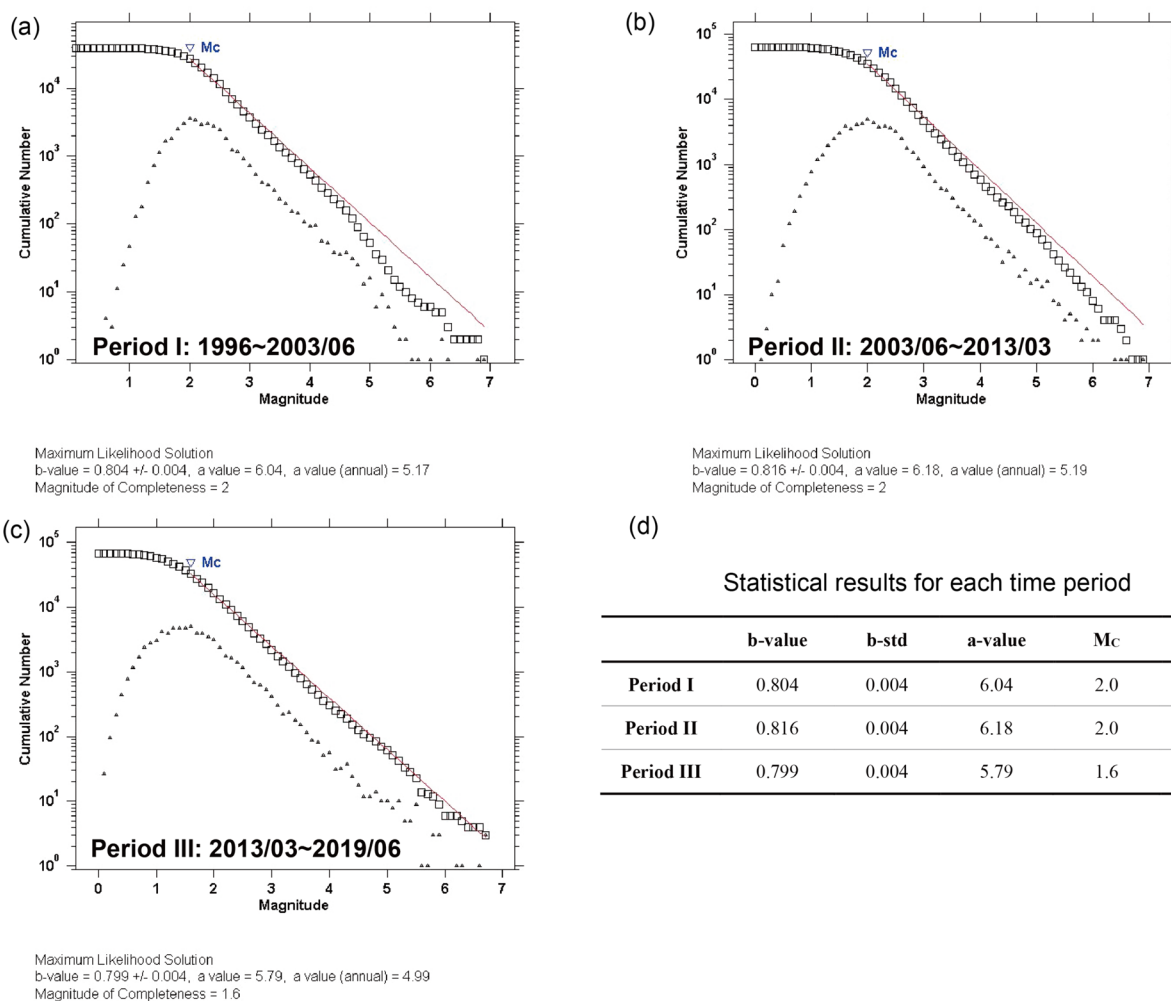


**Fig. 5** **a** Frequency–magnitude plot for period I; **b** frequency–magnitude plot for period II; **c** frequency–magnitude plot for period III; **d** statistical results for each period

degree of fitting with the cumulative number of earthquakes, and the standard deviation is small, indicating high reliability. As illustrated in Fig. 5d, from period I to period III, the  $b$  value and  $a$  value first increase and then decrease. Thus, from period I to period II, energy was released by earthquakes in eastern Taiwan, causing a slight increase in the  $b$  value. From period II to period III, the  $b$  value decreases to 0.799, and the  $a$  value also drops sharply, indicating a significant decrease in seismicity. The reduced number of earthquakes may indicate that the stress energy within the crust rapidly accumulates during this period.

The spatial distribution of  $b$  values from depth ranging from 0 to 70 km are illustrated in Fig. 6. Figure 6a shows the spatial distribution and the related standard deviations for period I. The lowest  $b$  value is approximately 0.627, and the low standard deviation distribution denotes high confidence. Low  $b$  values are located in the northern LV and offshore eastern Taiwan, varying in the NW–SE direction. Four large earthquakes occurred offshore during this period. Seismic events with a magnitude  $\geq 4$  mainly occurred near the coast in the northern Hualien area (indicated by white circles). Figure 6b presents the seismic  $b$  values and the related standard deviations in period II. The average  $b$  value is 0.816, with the lowest  $b$  value being 0.558. During this period, most areas show low standard deviations, and only the northern boundary of the study area shows higher values. The  $b$  value along the LVF is generally higher than that in period I. Notably, locations of earthquakes with a magnitude  $> 6$  were mainly distributed along the low  $b$  value area of period I, and seismic events with a magnitude  $\geq 4$

mainly still occurred offshore of eastern Taiwan. It is worth noting that the central LVF, near the Ruisui area begin to show lower  $b$  value at period II. The variations in seismic  $b$  value and the related standard deviation in period III are illustrated in Fig. 6c. The average  $b$  value during this period is 0.799, while the lowest value is 0.470. Most regions during this period also exhibit low standard deviations, demonstrating high reliability. During this period, the  $b$  values decrease more substantially than during the previous two periods, especially along the LVF and offshore eastern Taiwan. Seismicity during this period also decreased substantially before the occurrence of the 2018 Hualien earthquake, indicating that stress was building up until the occurrence of this earthquake. Furthermore, we observed that for all three time periods, most events greater than 6 occurred in the low  $b$  value region.

### 3.2 Seismic $b$ value profiles

Regarding the cross sections, the choosing conditions are close to the three epicenters and within the aftershock activity range of its mainshock. However, the goal of our selection is to discover the depth changes of the  $b$  value in the seismogenic areas of these earthquakes. In this section, we examine  $b$  value profiles across the LVF (AA'; BB'; CC') and along the fault (DD'). The location of each profile is displayed in Fig. 7. Figure 8a illustrates  $b$  value profiles from south to north across the LVF during period I. Several features are visible from the EW running profiles. First, beneath the MLF, the LDF, as well as the LCF, an east-dipping low  $b$  value region exists. Moving from north to south, seismic events with a magnitude greater

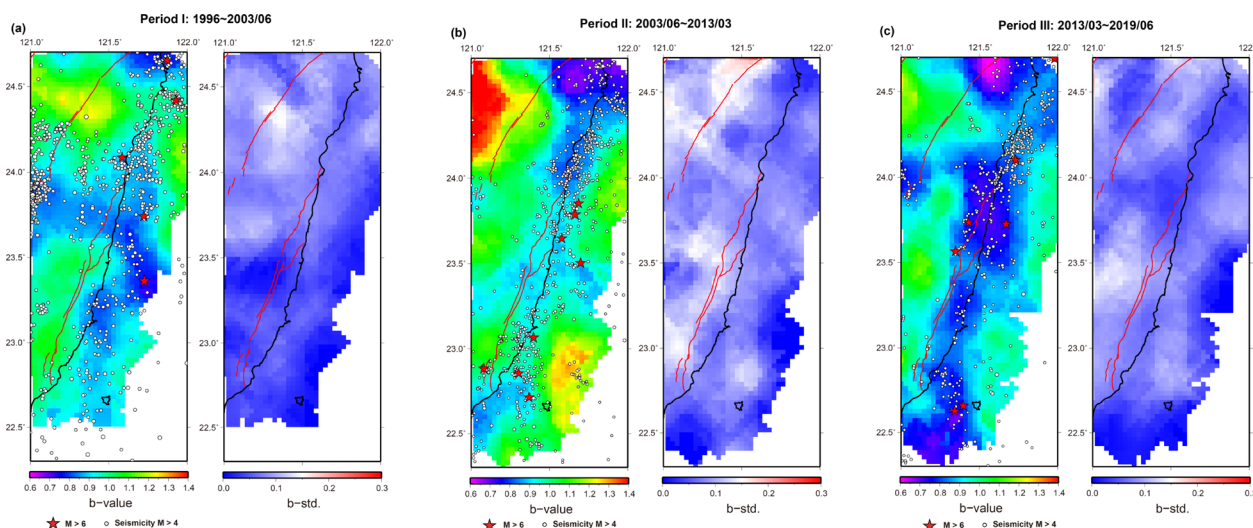


**Fig. 6** Temporal variations of seismic  $b$  values in east and offshore Taiwan. The left panel illustrates  $b$  value distribution, and the right panel represents standard deviation for (a) period I, (b) period II, and (c) period III

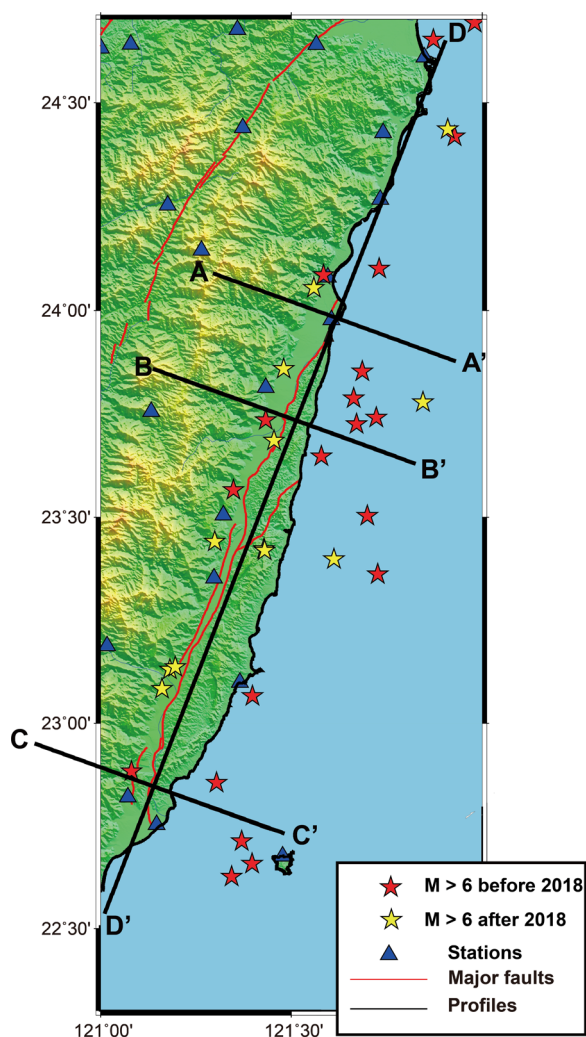


**Fig. 7** Locations of profiles AA', BB', and CC' across the LVF and profile DD' along the LVF

than 5 (indicated by larger white circles) all occurred in the low  $b$  value region, except for profile BB'. Several seismic events in the region exhibited a  $b$  value ranging from 0.9 to 1.0. Figure 8b shows the corresponding  $b$  value profiles during period II. The depth of the low  $b$  value region ranges from 40 to 50 km. The low  $b$  value region maintains an east-dipping trend in the profiles perpendicular to the LVF. Notably, a low  $b$  value region exists from a depth of 30 to 60 km, indicating stress heterogeneity at deeper depth. The low  $b$  value region persists right beneath the MLF, the LDE, and the LCF from north to south. These features suggest a somewhat connection between the low  $b$  value region and the fault zones. Finally, Fig. 8c presents the  $b$  value profiles for period III. As observed, all profiles exhibit a prominent low  $b$  value over a much broader area. For the profile along the LVE, the low  $b$  value feature extends to a depth of 70 km

especially in the north. Overall, the profiles along the LVE during the three periods show a significant low  $b$  value in the middle part of the LVE, where the RSF and YLF are located. Especially, during period III, the  $b$  value for this area is much lower than in the previous two periods. This feature may indicate a significant change in the stress state in a location where the seismic potential is high.

#### 4 Implications

The 2018 Hualien earthquake caused significant damage and casualties in Hualien city, making it one of the most notable seismic events since the 1951 earthquake sequence (Chen et al. 2008). Here, we inspect the stress state prior to the 2018 Hualien earthquake. Figure 9 illustrates the distribution of  $b$  values for period III, which includes  $M > 6$  events after 2018 (Table 1). These earthquakes are all distributed along the low  $b$  value areas in eastern Taiwan. In addition, Chen et al. (2023) precisely pointed out the  $b$  value anomaly just days before the occurrence of the 2018 Hualien earthquake, which is an important precursor. Although our  $b$  map shows years before the occurrence of the 2018 Hualien earthquake, our results are consistent with their findings, that is low  $b$  value indicates future occurrence of a large earthquake. However, two prominent low  $b$  value regions are clearly indicated in the northern and the middle of the LVF near the Ruisui area where the area is locked (e.g. Huang and Wang 2022) with low energy release (Fig. 2), which may indicate future rupture of a large earthquake and offshore eastern Taiwan. In addition, one possible interpretation regarding the correlation of low energy and low  $b$  value in the central Longitudinal Valley is that there is a long time that no large earthquake occurs near the Ruisui area till the 2013 Ruisui earthquake occurred, which leads to low energy release. In addition, low  $b$  value also imply high stress concentration, which can indicate that for future rupture of a large earthquake. Furthermore, subsequent to the 2018 Hualien earthquake, the majority of seismic events during the 2022 Hualien earthquake swarm occurred along the LDE, the northern segment of the LVE, which is characterized by lower  $b$  values. Moreover, the 2022 damaging Yuli earthquake ( $M_L$  6.6), which caused significant damage, occurred precisely in the central region with lower  $b$  values offshore eastern Taiwan (Fig. 9).

The seismic  $b$  value analysis conducted in eastern and offshore Taiwan generally indicates that a low seismic  $b$  value corresponds to a smaller number of large earthquake events, while a high seismic  $b$  value corresponds to a larger number of smaller earthquakes. Furthermore, a low  $b$  value region can be referred as an asperity directly. Scholz (2015) and Wu et al. (2018) remarked the  $b$  value is related to stress state of a region. With the definition of an asperity is an area with high stress. Sobiesiak et al.



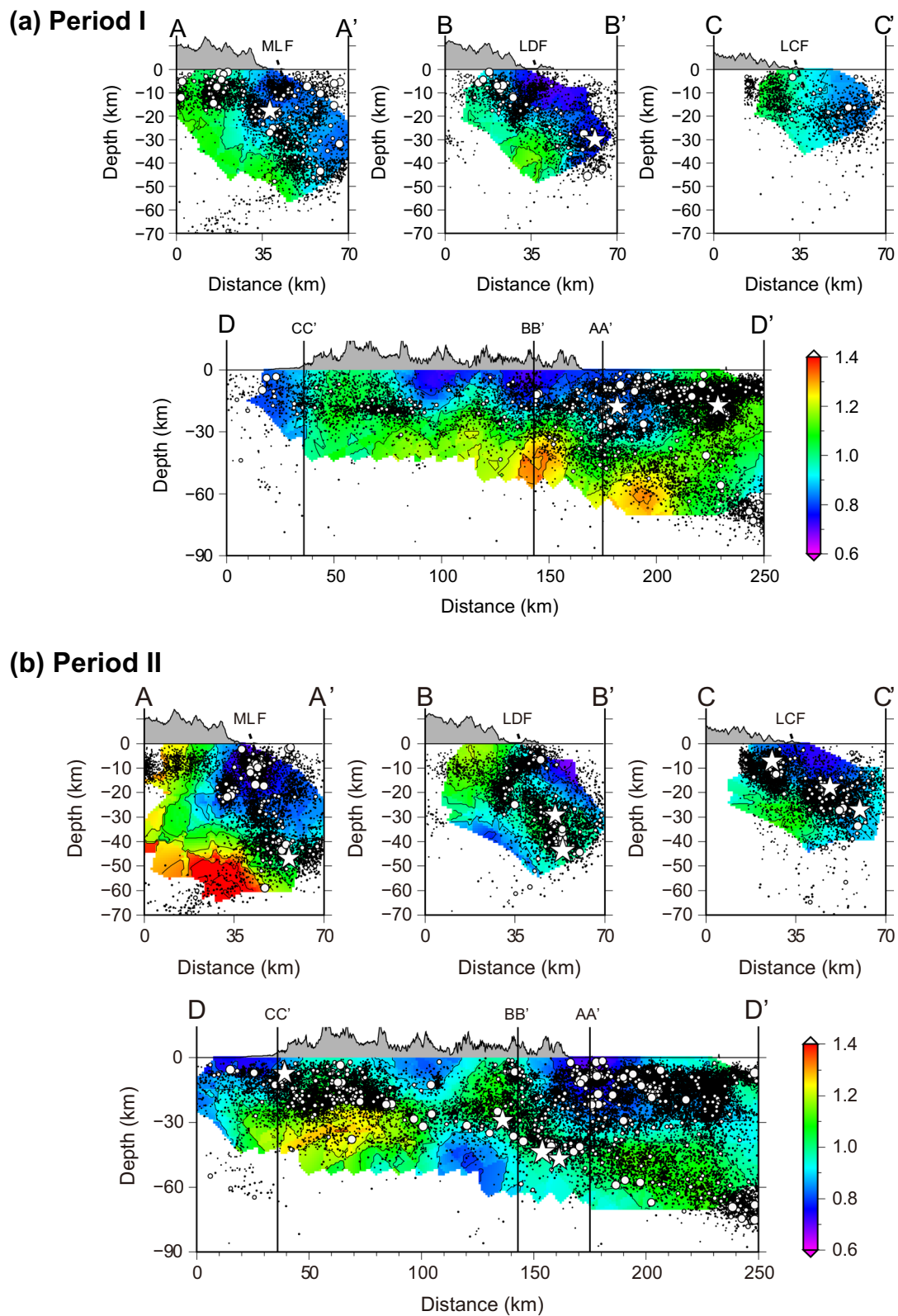


**Fig. 8** **a** Seismic  $b$  values cross sections for period I; **b** seismic  $b$  value cross sections for period II; **c** seismic  $b$  value cross sections for period III. Smaller circles indicate  $4 \leq M < 5$  events, and larger circles represent  $5 \leq M < 6$  events. White stars denote events with a magnitude greater than 6

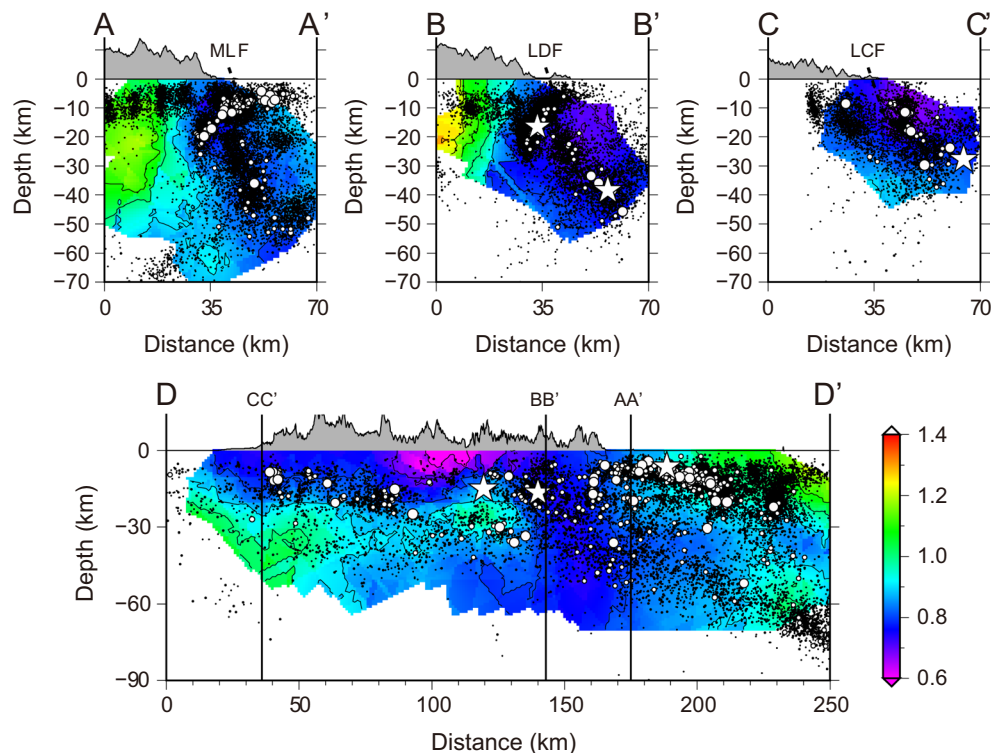
**(c) Period III**

Fig. 8 continued

(2007) and Wimer and Wyss (1997) also mentioned that an asperity is corresponding to low  $b$  value anomaly.

In addition, the seismic  $b$  value is depth-dependent, with a pronounced asperity observed in the north of the LVF at shallow depths (profile D–D', in period I and period II) and another asperity located in the middle of the LVF at greater depths, as depicted along profile D–D' during period II and period III. Spatial–temporal variations in seismic  $b$  values reveal a segmentation, indicating varying stress states along the LVF and offshore Taiwan from north to south. The strong asperities are located in the north and the central part of eastern Taiwan, which are classified as locking zones. Notably, the spatial variations of  $b$  values before the occurrence of the 2018 Hualien earthquake reveal two prominent asperities in the north and middle of the LVF and offshore Taiwan. As shown in Fig. 9, after the 2018 Hualien earthquake, three events occurred in the Yuli area, precisely within the asperity. In 2022 alone, nine earthquakes with a magnitude greater than 6 occurred in the study area (Fig. 9). This phenomenon indicates an unusual energy release situation, as indicated by the distribution of  $b$  values (see Figs. 6c and 8c). Another major fault in the LVF system is the west-dipping Central Range Fault (CRF), whose surface fault trace is not clearly evident and whose precise location

remains contentious. The CRF is considered to represent the boundary between the CMR and the LV. In addition, seismic tomography reveals a complex geometry of the boundary between the CMR and the Luzon volcanic arc system, which varies slightly from south to north. The boundary may not necessarily correspond to the foot of the eastern edge of the CMR on the surface. Geological surveys and geophysical data suggest that it may be a blind fault, particularly in the northern section of the LV. However, findings from the Guanshan–Chishang earthquake sequence in 2022 indicate a close relationship between its rupture and the CRF (Lee et al. 2023). Furthermore, based on the recent  $b$  value distribution depicted in Fig. 6c, the CRF is situated in the low- $b$  value region. Consequently, the CRF emerges as a pivotal seismogenic structure in eastern Taiwan that warrants close monitoring.

## 5 Conclusions

The eastern region of Taiwan is located at the junction of the Eurasian Plate and the Philippine Sea Plate and experiences severe seismic activity. A historical analysis of earthquakes in Taiwan highlights the prevalence of significant seismic events in this region. Based on the seismic  $b$  values and the seismogenic characteristics of

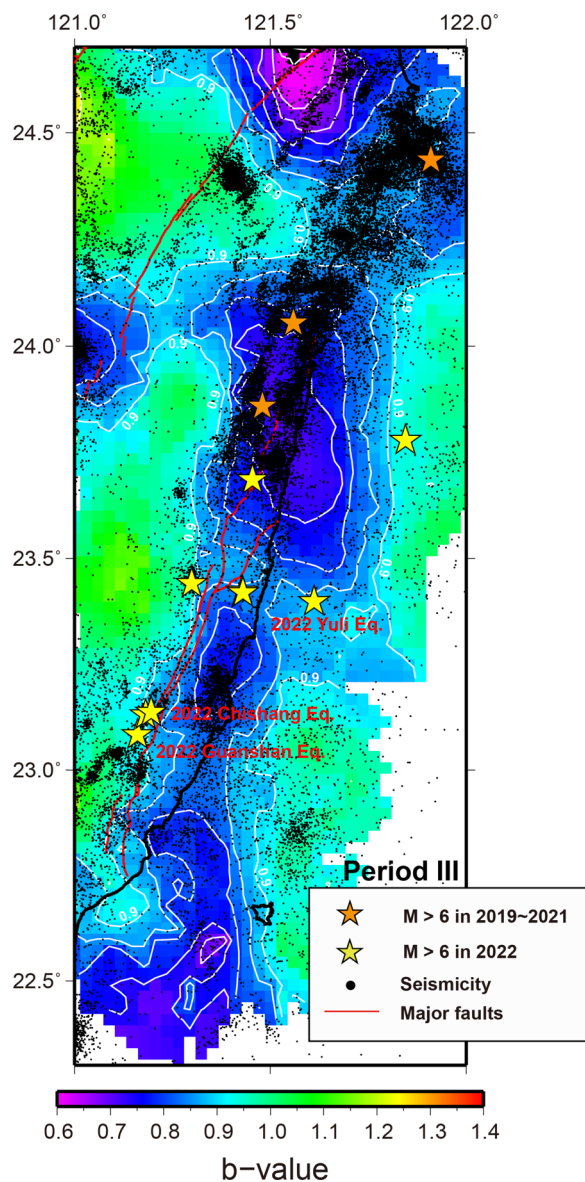


**Fig. 9** Spatial variations of seismic  $b$  values (period III) prior to the occurrence of the 2019–2022 events. The line with a contour of 0.9 has been marked. From the distribution diagram in the figure, it can be seen that most of the M6+ events are located in the range where the  $b$  value is less than 0.9

eastern Taiwan, the main conclusions of this study are as follows:

1. Epicenters of earthquakes with magnitudes greater than 5 typically overlap with areas exhibiting low  $b$  values (the larger the magnitude, the higher the degree of overlap), indicating that regions with lower  $b$  values generally have a higher probability of larger magnitude seismic events.
2. The spatial–temporal distribution map of  $b$  values in eastern Taiwan during period III indicates that the stress state near the MLF and the LDF is complex, considering that numerous medium to large earthquakes have occurred in the past. Because the occurrence is frequent, the seismic  $b$  value of the most recent period is low, making it a high-risk area, meaning that this is a high-risk zone.
3. The DD' section in period III reveals a low  $b$  value area underneath the CSF, the RSF, the YLF and the Chimei Fault. The current activity around the CSF pertains to creeping faults. Most cases involve high  $b$  value characteristics. The possible reason is that the environment of no-seismic slip or micro-earthquakes extends for long periods and that the number of surrounding seismic stations is insufficient to detect small earthquakes from submerged faults, resulting in low  $b$  values. In addition to this area, the low  $b$  value region between the LCF and Green Island poses a potential threat for future catastrophic earthquakes. Furthermore, the region beneath the RSF and the YLF exhibits the lowest  $b$  value, indicating high seismic potential that warrants close attention.
4. The  $b$  value estimation in this study still remain robust when slightly changes are made to the criterion for determining  $b$  values.

#### Acknowledgements

The authors would like to thank the Central Weather Administration, which provides seismic catalogue (GDMS, <https://gdmsn.cwa.gov.tw/index.php>). We also like to express our gratitude to Dr. Honn Kao and anonymous reviewers for their constructive feedback, which has significantly improved the quality of the manuscript. This research is supported by NSTC 113-2116-M-194-011.

#### Author contributions

YLY interpreted the data and results and manuscript writing, BYH did data acquisition and data processing, SW initiated the project, interpreted the results, manuscript writing and manuscript revisions.

#### Data availability statement

The data is available upon request.

#### Declaration

#### Conflict of interest

The authors declare that they have no conflict of interest.

#### Author details

<sup>1</sup>Department of Earth and Environmental Sciences, National Chung Cheng University, 168 University Road, Min-Hsiung, Chia-Yi 62102, Taiwan. <sup>2</sup>Southern Taiwan Earthquake Center, National Chung Cheng University, Chiayi, Taiwan.

Received: 28 March 2024 Accepted: 9 September 2024  
Published online: 26 September 2024



## References

- Angelier J, Chu HT, Lee JC, Hu JC (2000) Active faulting and earthquake hazard: the case study of the Chihshang Fault, Taiwan. *J Geodyn* 29:151–185. [https://doi.org/10.1016/S0264-3707\(99\)00045-9](https://doi.org/10.1016/S0264-3707(99)00045-9)
- Chan CH, Wu YM, Tseng TL, Chen CC (2012) Spatial and temporal evolution of *b*-values before large earthquake in Taiwan. *Tectonophysics* 532–535:215–222
- Chen KH, Shinji T, Rau RJ (2008) A leaping, triggered sequence along a segmented fault: the 1951 ML 7.3 Hualien-Taitung earthquake sequence in eastern Taiwan. *J Geophys Res* 113:B02304. <https://doi.org/10.1029/2007J1B005048>
- Chen HY, Tung H, Hsu YJ, Lee HK (2020) Evaluation of single-frequency receivers for studying crustal deformation at the longitudinal Valley fault, eastern Taiwan. *Surv Rev* 52(374):454–462. <https://doi.org/10.1080/00396265.2019.1634340>
- Chen SK, Chen PY, Wu YM, Chen CC, Chan CH (2023) Temporal variations of earthquake magnitude-frequency relation in the source area of  $M \geq 6.0$  earthquakes: a systematic survey in Taiwan. *Earth Space Sci* 10:e2023EA002927. <https://doi.org/10.1029/2023EA002927>
- Cheng SN, Yeh YT (1989) Catalogue of earthquakes in Taiwan from 1604 to 1988. Open-File Report. Inst Earth Sci, Acad Sin, 255 pp. (in Chinese)
- Cheng SN, Yeh YT, Yu MS (1996) The 1951 Taitung Earthquake in Taiwan. *J Geol Soc China* 39(3):267–285
- Farrell J, Husen S, Smith RB (2009) Earthquake swarm and *b*-value characterization of the Yellowstone volcano-tectonic system, *J Volcanol Geotherm Res* 188:260–276
- Gerstenberger M, Wiemer S, Giardini D (2001) A systematic test of the hypothesis that *b* varies with depth in California. *Geophys Res Lett* 28(1):57–60
- Gulia L, Tormann T, Wiemer S, Herrmann M, Seif S (2016) Short-term probabilistic earthquake risk assessment considering time dependent *b* values. *Geophys Res Lett* 43:1100–1108. <https://doi.org/10.1002/2015GL066686>
- Gutenberg R, Richter CF (1944) Frequency of earthquakes in California. *Bull Seismol Soc Am* 34:185–188
- Huang HH, Wang Y (2022) Seismogenic structure beneath the northern Longitudinal Valley revealed by the 2018–2021 Hualien earthquake sequences and 3D velocity model. *Terr Atmos Ocean Sci* 33:17. <https://doi.org/10.1007/s44195-022-00017-z>
- Huang WJ, Johnson KM, Fukuda J, Yu SB (2010) Insight into active tectonics of eastern Taiwan from analysis of geodetic and geological data. *J Geophys Res* 115:B03413. <https://doi.org/10.1029/2008JB006208>
- Hui C, Cheng C, Ning L, Yang J (2020) Multifactorial characteristics of seismogenic systems and *b* values in the Taiwan Seismic Region. *ISPRS Int J Geo-Inf* 9(6):384. <https://doi.org/10.3390/ijgi9060384>
- Kim KH, Chang CH, Ma KF, Chiu JM, Chen KC (2005) Modern seismic observation in the Tatun volcano region of northern Taiwan: seismic/volcanic hazard adjacent to the Taipei metropolitan area. *Terr Atmos Ocean Sci* 16:579–594
- Lee CP, Kim KH, Huang BS, Huang WG (2011) Seismicity, active faults, stress patterns, and rupture processes in the Hualien region, Taiwan, investigated using the 1990 Hualien earthquake sequence. *Tectonophysics* 511:27–37
- Lee SJ, Liu TY, Lin TC (2023) The role of the west-dipping collision boundary fault in the Taiwan 2022 Chihshang earthquake sequence. *Sci Rep* 13:3552
- Marzocchi W, Sandri L (2003) A review and new insights on the estimation of the *b*-value and its uncertainty. *Ann Geophys* 46(6):1271–1282
- Mazzotti O, Leonard LJ, Cassidy JF, Rogers GC, Halchuk S (2011) Seismic hazard in western Canada from GPS strain rate versus earthquake catalog. *J Geophys Res* 116:B12310. <https://doi.org/10.1029/2011JB008213>
- Mignan A (2015) Modeling aftershocks as a stretched exponential relaxation. *Geophys Res Lett* 42:9726–9732. <https://doi.org/10.1002/2015GL066232>
- Nanjio KZ, Yoshida AA (2018) *b* Map implying the first eastern rupture of the Nankai Trough earthquakes. *Nat Commun* 9:11. <https://doi.org/10.1038/s41467-018-03514-3>
- Okal EA (2019) Energy and magnitude: a historical perspective. *Pure Appl Geophys* 176:3815–3849. <https://doi.org/10.1007/s00024-018-1994-7>
- Peyret M, Dominguez S, Cattin R, Champenois J, Leroy M, Zajac A (2011) Present day interseismic surface deformation along the longitudinal Valley, eastern Taiwan, from a PS-InSAR analysis of the ERS satellite archives. *J Geophys Res* 116:B03402. <https://doi.org/10.1029/2010JB007898>
- Raub C, Patricia MG, Grzegorz K, Marco B, Georg D (2017) Variations of seismic *b*-value at different stages of the seismic cycle along the North Anatolian Fault Zone in northwestern Turkey. *Tectonophysics* 712–713:232–248. <https://doi.org/10.1016/j.tecto.2017.05.028>
- Reasenberg P (1985) Second-order moment of central California seismicity. *J Geophys Res* 90:5479–5495. <https://doi.org/10.1029/JB090iB07p05479>
- Scholz CH (2015) On the stress dependence of the earthquake *b* value. *Geophys Res Lett* 42:1399–1402. <https://doi.org/10.1002/2014GL02863>
- Schurr B, Asch G, Hainzl S, Bedford J, Hoechner A, Palo M, Wang R, Moreno M, Bartsch M, Zhang Y, Oncken O, Tilmann F, Dahm T, Victor P, Barrientos S, Vilotte JP (2014) Gradual unlocking of plate boundary controlled initiation of the 2014 Iquique earthquake. *Nature*. <https://doi.org/10.1038/nature13681>
- Sobiesiak MM, Meyer U, Schmidt S, Götze HJ, Krawczyk C (2007) Asperity generating upper crustal sources revealed by *b*-value and isostatic residual anomaly grids in the area of Antofagasta. *J Geophys Res* 112:B12308. <https://doi.org/10.1029/2006JB004796>
- Theunissen T, Font Y, Lallemand S, Liang WT (2010) The largest instrumentally recorded earthquake in Taiwan: revised location and magnitude, and tectonic significance of the 1920 event. *Geophys J Int* 183:1119–1133. <https://doi.org/10.1111/j.1365-246X.2010.04813.x>
- Tormann T, Wiemer S, Mignan A (2014) Systematic survey of high-resolution *b* value imaging along Californian faults: inference on asperities. *J Geophys Res* 119:2029–2054. <https://doi.org/10.1002/2013JB010867>
- Tormann T, Enescu B, Woessner J, Wiemer S (2015) Randomness of megathrust earthquakes implied by rapid stress recovery after the Japan earthquake. *Nat Geosci* 8:152–158. <https://doi.org/10.1038/NGEO2343>
- Tsai YB, Liaw ZS, Lee TQ (1981) A statistical study of the Taiwan telemetered seismographic network data during 1973–1979. *Bull Inst of Earth Sci, Acad Sin* 1:1–22
- Wang JH (1988) *b*-values of shallow earthquakes in Taiwan. *Bull Seismol Soc Am* 78(3):1243–1254. <https://doi.org/10.1785/BSSA0780031243>
- Wang JH, Chen KC, Leu PL, Chang JH (2015) *b*-Values observations in Taiwan: a review. *Terr Atmos Ocean Sci* 26:475–492
- Wang YJ, Chan CH, Lee YT, Ma KF, Shyu JBH, Rau RJ, Cheng CT (2016) Probabilistic seismic hazard assessment for Taiwan. *Terr Atmos Ocean Sci* 27:325–340
- Wen YY, Chen CC, Wen S, Lu WT (2022) Spatiotemporal seismicity pattern of the Taiwan orogeny. *Nat Hazards Earth Syst Sci* 23:1835–1846. <https://doi.org/10.5194/nhess-2022-242>
- Wiemer S (2001) A software package to analyze seismicity: ZMAP. *Seismol Res Lett* 72:373–382
- Wiemer S, Wyss M (1997) Mapping the frequency-magnitude distribution in asperities: an improved technique to calculate recurrence times? *J Geophys Res* 102(B7):15115–15128. <https://doi.org/10.1029/97JB00726>
- Wiemer S, Wyss M (2000) Minimum magnitude of complete reporting in earthquake catalogs: examples from Alaska, the Western United States, and Japan. *Bull Seismol Soc Am* 90:859–869. <https://doi.org/10.1785/0119990114>
- Wiemer S, McNut SR, Wyss M (1998) Temporal and three-dimensional spatial analyses of the frequency-magnitude distribution near Long Valley Caldera, California. *Geophys J Int* 134:409–421
- Wu YH, Chen CH, Turcotte DL, Rundle JB (2013) Quantifying the seismicity on Taiwan. *Geophys J Int* 194:465–469
- Wu YM, Chen SK, Huang TC, Huang HH, Chao WA, Koulikov I (2018) Relationship between earthquake *b*-values and crustal stresses in a young orogenic belt. *Geophys Res Lett* 45:1832–1837. <https://doi.org/10.1002/2017GL076694>
- Wyss M, Schorlemmer D, Wiemer S (2000) Mapping asperities by minima of local recurrence time: the San Jacinto-Elsinore fault zones. *J Geophys Res* 105:7829–7844. <https://doi.org/10.1029/1999JB000347>
- Yadav RBS, Bormann P, Rastogi BK, Das MC, Chopra S (2009) A homogeneous and complete earthquake catalog for northeast India and the adjoining region. *Seismol Res Lett* 80:609–627. <https://doi.org/10.1785/gssrl.80.4.609>
- Yeh YL, Wen S, Chang CH (2021) Tectonic implications of the deformation front in southwest Taiwan: revealed by 3D seismic *b* values. *Pure Appl Geophys* 178:1631–1641. <https://doi.org/10.1007/s00024-021-02721-2>
- Yu SB, Kuo LC (2001) Present-day crustal motion along the Longitudinal Valley fault, eastern Taiwan. *Tectonophysics* 333:199–217
- Yu SB, Lee CW (1986) Geodetic measurement of horizontal crustal deformation in eastern Taiwan. *Tectonophysics* 125:73–85
- Zhao YZ, Wu ZL (2008) Mapping the *b*-values along the Longmenshan fault zone before and after the 12 May 2008, Wenchuan, China,  $M_s$  8.0 earthquake. *Nat Hazards Earth Syst Sci* 8:1375–1385
- Zhou Y, Zhou S, Zhong J (2018) A test on methods for MC estimation based on earthquake catalog. *Earth Planet Phys* 2:150–162

### **Publisher's Note**

Springer Nature remains neutral with regard to jurisdictional claims in published maps and institutional affiliations.